

Chapter 6

Coherent Structures and Flux Coupling

Christoph K. Thomas, Andrei Serafimovich, Lukas Siebicke, Tobias Gerken,
and Thomas Foken

6.1 Introduction

Coherent structures in the atmosphere are one important canopy flow mode in the roughness sublayer of forests of any architecture as they have the ability to transport energy and matter over long distances in a spatially coherent fashion (Gao et al. 1989; Shaw et al. 1989; Paw U et al. 1992; Thomas and Foken 2007a). Their importance for the horizontal and vertical transport and exchange in forest canopies

C.K. Thomas (✉)

University of Bayreuth, Micrometeorology Group, 95440 Bayreuth, Germany

Bayreuth Center of Ecology and Environmental Research, University of Bayreuth, Bayreuth, Germany

e-mail: christoph.thomas@uni-bayreuth.de

A. Serafimovich

Helmholtz-Zentrum Potsdam, Deutsches GeoForschungsZentrum GFZ, Telegrafenberg, Haus A 6, 14473 Potsdam, Germany

L. Siebicke

Department of Bioclimatology, Georg-August University of Göttingen, Büsingenweg 2, 37077 Göttingen, Germany

T. Gerken

Department of Land Resources and Environmental Sciences, Montana State University, 334 Leon Johnson Hall, Bozeman, MT 59717, USA

T. Foken

Am Herrgottsbaum 28, 96120 Bischberg, Germany

Bayreuth Center of Ecology and Environmental Research, University of Bayreuth, Bayreuth, Germany

C. K. Thomas, L. Siebicke, A. Serafimovich, T. Gerken, and T. Foken: Affiliation during the work at the Waldstein sites – University of Bayreuth, Department of Micrometeorology, Germany

arises from the fact that the associated velocity perturbations are substantially stronger compared to the other common flow modes including the ubiquitous stochastic “background” turbulence, von Kármán vortices shed by canopy elements such as tree trunks and branches, the submeso-scale modes (Thomas 2011), canopy waves (Cava et al. 2004), and boundary-layer scale convective eddies (Poggi et al. 2004; Thomas et al. 2006). Coherent structures are commonly referred to as “organized motions,” which expresses that individual motions have distinct and predictable temporal and spatial scales including a quasi-stationary arrival frequency, as opposed to the random stochastic motions, which can only be described in terms of their ensemble probability density function. The terminology of “coherent structures” in atmospheric flows is ambiguous in the literature and has been used to describe a variety of flow phenomena resulting from a variety of generating mechanisms (see overview in Kallistratova and Kouznetsov 2004).

For the purpose of this chapter focusing on flow phenomena and flux coupling in plant canopies, we define a coherent structure as a spatially coherent motion whose length and vertical dimensions scale with the density and depth of the vegetated canopy. In vector time series, they occur as a fairly symmetric triangle-like pattern, whereas in scalar time series, they have an asymmetric ramp-like shape (Thomas and Foken 2007b). The physical process connected with one event can be separated into an initial upward motion (ejection, burst) followed by a rapid downward motion (sweep, gust). The temporal scale varies from several seconds up to a few minutes.

Based on the similarity of structural characteristics of coherent structures in the atmosphere under varying stability conditions, Gao et al. (1989) identified the vertical wind shear as the main generating mechanism of coherent structures. The results of Paw et al. (1992) supported this finding by demonstrating a functional relationship between the occurrence frequency of coherent structures and the canopy shear scale $U_{hc}h_c^{-1}$, where U_{hc} is the mean horizontal wind speed at the canopy height, h_c . Raupach et al. (1996) continued to investigate coherent structures in the forest air layer and proposed a theory for their generation in neutral stratification called the mixing-layer analogy. This theory states that if the above-canopy and canopy air layers are allowed to mix, a mixing layer develops in which coherent structures form in the atmosphere as a result of flow instabilities created at the height of the maximum vertical shear, i.e., the inflection point of the horizontal velocity profile. The initial phase of their evolution can be described as a hairpin vortex that may organize into larger-scale structures (Zhou et al. 1999; Hommema and Adrian 2003; Adrian 2007).

While coherent structures have been investigated by a large number of authors across a wide spectrum of forest and agricultural canopies, the coherent structures’ research conducted at the Waldstein site contributed three important aspects to this field of research: firstly, the development of a refined automated and largely objective detection algorithm based upon pattern recognition algorithms using the wavelet transformation; secondly, the definition of a set of distinct exchange regimes, which allows for a categorization of the varying degrees of vertical and horizontal coupling between the sub-canopy, canopy, and above-canopy air layers by coherent structures; and thirdly, an alternative explanation for the occurrence

of systematic spatial CO_2 concentration gradients and thus sub-canopy horizontal advection by linking the horizontal and vertical exchange regimes with the spatial distribution of plant area density.

In this chapter, we will focus on these abovementioned aspects rather than providing a comprehensive review of coherent structures in forest canopies. Our goal is to provide a synthesis of the novel aspects in research on coherent structures connected to the Waldstein experimental site from peer-reviewed publications and unpublished academic theses. The overarching objectives of analyzing coherent structures at this site are to improve our understanding of the dynamic turbulent exchange process at the plant-air interface, to reduce uncertainty in flux estimates of energy and matter, and to utilize the specific information about the exchange process to partition the net carbon exchange and gauge their impact on horizontal gradients and advection. The reader is referred to Appendix A to find information about the dates and experimental setups of field experiments and campaigns references in this chapter.

6.2 Materials and Methods

6.2.1 Detection Algorithm and Conditional Flux Computation

Here, we will briefly review the analytical method presented by Thomas and Foken (2005) to extract individual coherent structures from the time series of vector components and scalars by means of conditional sampling with the goal of computing their ensemble averaged statistics including duration and arrival frequency [Figs. 6.1 and 6.2 from Thomas and Foken (2005) and Zeeman et al. (2013), respectively]. In a subsequent step, the flux contribution of the ejection and sweep phases and that of the total coherent structure can be computed by applying a triple decomposition to the conditionally sampled time series (Antonia et al. 1987; Bergström and Högström 1989; Thomas and Foken 2007a).

As a first step, outliers in high-frequency time series are removed using a despiking method (Vickers and Mahrt 1997) with a window length of 300 s and an initial threshold criterion of 6.5 standard deviations (σ) repeated iteratively a maximum number of ten times to prepare the observed signals for analysis. This test detects and removes spikes while preserving the sharply localized instationarities commonly associated with coherent structures. Vector components are rotated using a sector-wise planar fit rotation (Wilczak et al. 2001) or double-rotation method (Thomas et al. 2013). Scalar time series are corrected for time lags compared to the vertical wind trace by shifting the time series until the vector-scalar covariance is maximized. To reduce the computation time needed for the subsequent wavelet analysis, signals are linearly block-averaged to a 2 Hz sampling resolution. This step does not significantly alter the statistical properties of the contained coherent structures as their time scales typically exceed tens of seconds. Any time series of quantity x is then normalized by subtracting the mean X and dividing by the

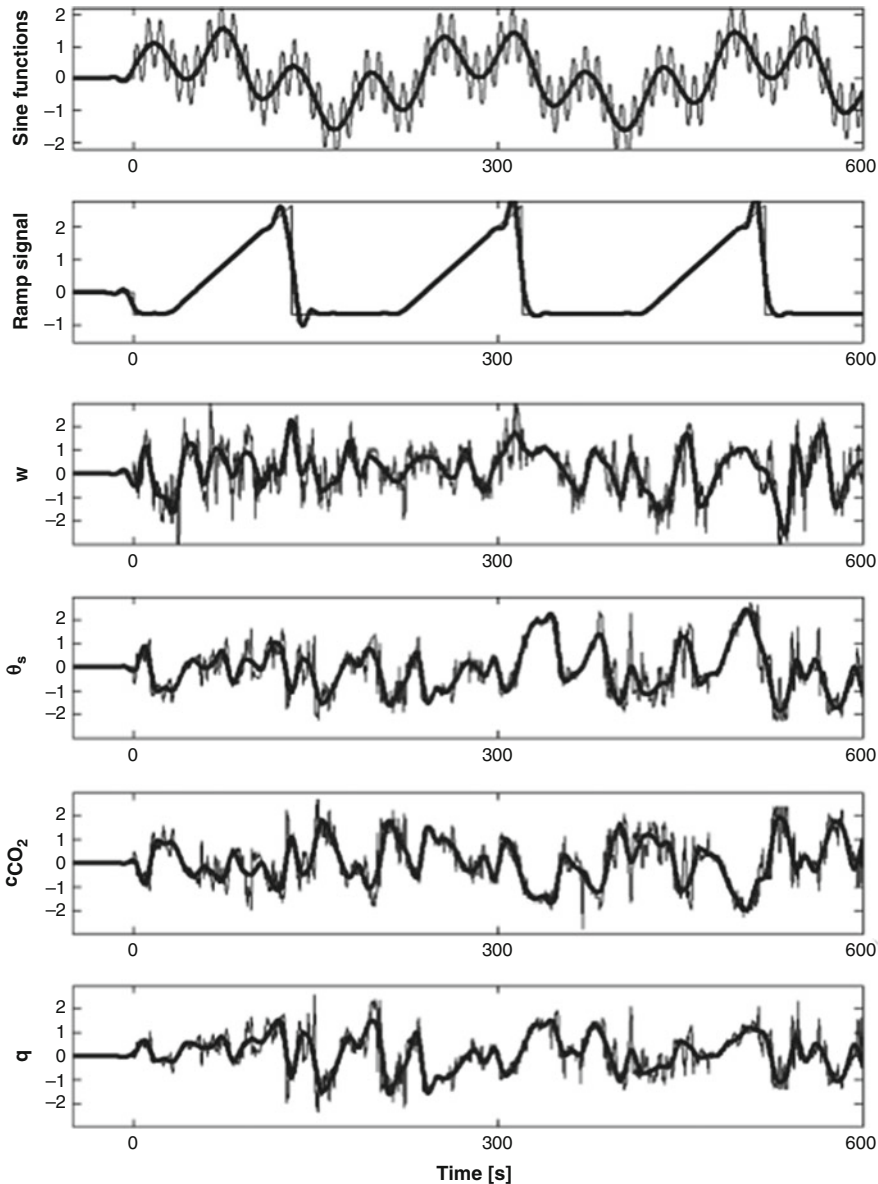


Fig. 6.1 Zero-padded extended and normalized original (*thin*) and low-pass filtered (*bold*) time series, which was block-averaged data to a resolution of 2 Hz for an artificial sinusoidal and ramp signals (*upper two panels*), and for observed time series of the vertical wind w , potential sonic temperature θ_s , carbon dioxide concentration c_{CO_2} , and specific humidity q (Adapted from Thomas and Foken (2005), with kind permission © Springer 2005, All rights reserved)

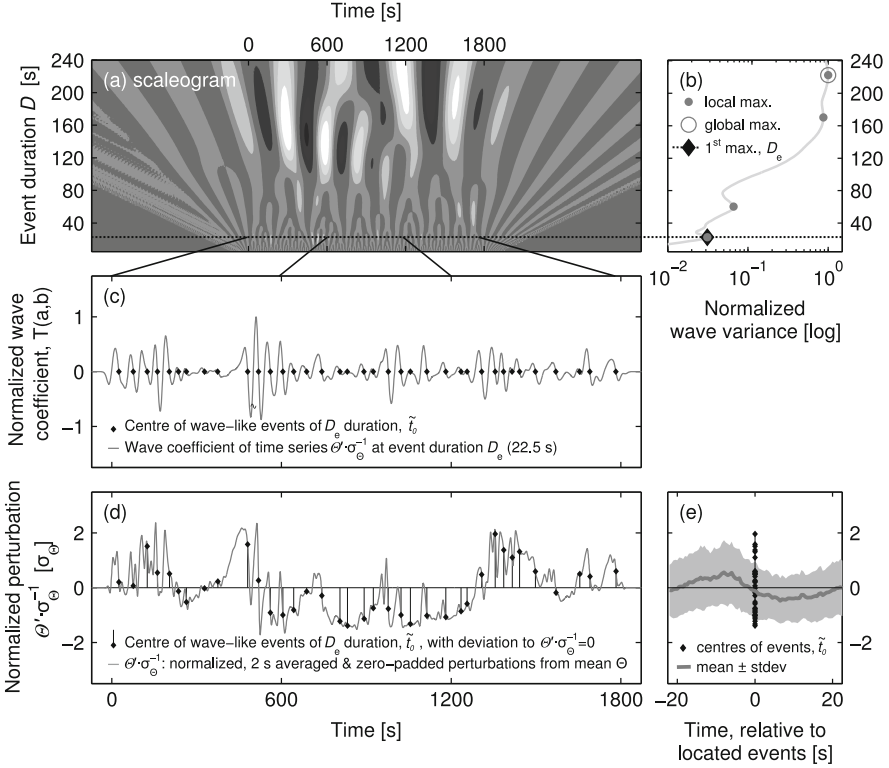


Fig. 6.2 An example of the application of the coherent structure detection methodology (Adapted from Zeeman et al. (2013), with kind permission © Springer 2013, All rights reserved) showing (a) the scalogram of wavelet coefficients expressed in brightness for the normalized air temperature perturbations (θ'), the (b) normalized wavelet variance and occurring variance maxima, the (c) normalized wavelet coefficients and the localization of events in time, the (d) time series of normalized air temperature perturbations θ' with indication of the localized events, and (e) the ensemble mean and standard deviation of the normalized θ' for these localized events within a $2D_e$ time window. The event duration D_e is determined from the first occurring variance maximum as shown in (b), which in this case is 22.5 s

standard deviation σ_x , except for the vertical wind w , which is normalized by $w_\sigma w^{-1}$ only. In a last step, time series are passed through a low-pass wavelet filter using the biorthogonal set of wavelets BIOR5.5 to filter out all small-scale high-frequency turbulence with event durations $D < D_c = 6.2$ s, where D_c is the critical event duration. D_c is determined from the turbulence spectrum and is thought to spectrally separate the small-scale stochastic turbulence from the longer-scale coherent structures. For practical purposes, it is assumed to be constant over time. The chosen value is in close agreement with that of other studies [$D_c = 5$ s in Lykossov and Wamser (1995), $D_c = 7$ s in Brunet and Collineau (1994), and $D_c = 5.7$ s in Chen and Hu (2003)]. We prefer this set of wavelet functions since its localization in frequency is better than, e.g., that of the HAAR wavelet (Kumar

and Foufoula-Georgiou 1994). The purpose of low-pass filtering the times series is to facilitate the detection of the spectral peak associated with coherent structures in the wavelet variance spectra.

After zero-padding the time series to avoid sharp instationarities at both ends, a continuous wavelet transformation is applied to the signal $f(t)$ using the complex Morlet wavelet as the analyzing mother wavelet (Fig. 6.2):

$$T_p(a, b) = \frac{1}{a^p} \int_{-\infty}^{+\infty} f(t) \Psi\left(\frac{t-b}{a}\right) dt \quad (6.1)$$

where $T_p(a, b)$ are the wavelet coefficients, a the dilation scale, and b the translation parameter and the normalization factor $p = 1$ in our case. The complex Morlet wavelet function is best localized in the frequency domain and well suited to determine the spectral peak associated with coherent structures. The duration scales D used for the wavelet transform ranges between 6 s and 240 s with a step width of 1 s. The event duration D can be linked to the dilation scale a of the wavelet transform (e.g., Collineau and Brunet 1993) by

$$D = \left(\frac{1}{2}\right) f^{-1} = \frac{a\pi}{f_s \omega_{\psi_{1,1,0}}^0}, \quad (6.2)$$

where f is the natural frequency corresponding to the event duration, f the sampling frequency of the time series, and ω_{ψ}^0 the center frequency of the mother wavelet function. For illustration purposes, the event duration D corresponds to half the period length of a sine function. The wavelet variance spectrum $W_p(a)$ is then computed as

$$W_p(a, b) = \int_{-\infty}^{+\infty} |T_p(a, b)|^2 db. \quad (6.3)$$

The characteristic event duration or temporal scale of coherent structures D_e was determined from scale a_e at which $W_p(a)$ exhibits its first spectral peak where the subscript “e” stands for event. Due to the local character of the wavelet transform, D_e corresponds to the characteristic event duration of coherent structures and not to their arrival frequency or periodicity (Howell and Mahrt 1997).

Applying another wavelet transformation at the previously determined event duration D_e using the Mexican-hat wavelet function allows for detection and extraction of individual coherent structures. Its wavelet coefficients $T_p(a_e, b)$ exhibit a zero-crossing along with a defined change in sign at the moment of occurrence (see Table 2 in Thomas and Foken 2005). Zero-crossings offer the advantage of being easily detected and avoid the need to define thresholds. The last step yields the individual moments of occurrence as well as the total number of detected coherent structures in a given time interval.

Expanding upon the classical Reynold’s decomposition of any instantaneous variable into its temporal mean and perturbation thereof, $x = X + x'$, the pertur-

bations can be subdivided into a portion contributed by the coherent structures and small-scale stochastic background turbulence, $x' = x_{cs} + x_t$, arriving at a triple decomposition (Antonia et al. 1987; Bergström and Högström 1989). If one samples a signal $x(t)$ using the detected moments of occurrence of coherent structures as the sampling condition and subsequently applies a conditional averaging operator $\langle \rangle$ over all subsamples, one obtains

$$\langle x' \rangle = \langle x_t \rangle, \quad (6.4)$$

where the right-hand term is the contribution of coherent structures to the fluctuation and $\langle x_t \rangle = 0$ under the assumption that coherent structures and small-scale turbulence are uncorrelated. Invoking Reynold's second postulate on the product of two arbitrary variables x and y and applying an averaging operator over the conditional sample given by

$$\widetilde{\langle x \rangle} = \frac{1}{2D_e} \int_{-D_e}^{+D_e} \langle x'(t) \rangle \delta t. \quad (6.5)$$

one can compute the total flux as

$$\widetilde{\langle x'y' \rangle} = \widetilde{\langle x' \rangle \langle y' \rangle} + \widetilde{\langle x_t y_t \rangle}, \quad (6.6)$$

where the left-hand term represents the total flux of the conditionally sampled region of the turbulent flow, the first term on the right-hand side is the flux contribution of coherent structures, and the second term is that of the small-scale stochastic turbulence. It is convenient to write Eq. 6.6 as

$$F(x, y)_{\text{tot}} = F(x, y)_{\text{cs}} + F(x, y)_t. \quad (6.7)$$

The flux contributions of the ejection phase F_{ej} and of the sweep phase F_{sw} are determined by applying the averaging operator in Eq. 6.5 within $[-D_e, 0]$ and $[0, +D_e]$, respectively, whereas $F_{\text{cs}} = F_{\text{ej}} + F_{\text{sw}}$. Assuming scalar similarity, all signals are sampled according to the events contained in the sonic temperature traces. This choice seems justified as (i) coherent structures were found to be well pronounced in T_s time series during day and night, and its use facilitates the comparison with other studies.

6.2.2 Adapted Experimental Setup

Diagnosing the vertical and horizontal flux of energy and matter and the degree of coupling in a forest canopy requires spatially explicit observations. These locations are expected to represent the flow dynamics in the main vertical canopy layers,

i.e., the sub-canopy layer or clear bole space, the tree crown layer, and the above-canopy layer, or to represent the horizontal canopy architecture for the main flow directions. The first will result in simultaneous measurements from sonic anemometers and trace gas analyzers in a vertical profile with at least three to five observational levels within the forest canopy (Thomas and Foken 2007a), with the latter adding horizontal transects of sub-canopy observations for the main wind directions (Serafimovich et al. 2011). Chapter 2 and Appendix A in this volume give an exhaustive description of the experimental setups used to investigate coherent structures at the Waldstein-Weidenbrunnen site, while here we mention only some key elements. Fast-response data from all sensors are collected at a sampling frequency f_s of at least 10 Hz to adequately capture the high-frequency stochastic turbulence. The time stamps of the data acquisition systems recording the fast-response data of the individual sensors need to be synchronized to be within $1/f_s$ to eliminate artifacts due to time lags. Only accurately recorded time stamps allow for tracking of individual coherent structures to determine their penetration depth with the goal of diagnosing vertical coupling and determination of their effective transporting velocities (Zeeman et al. 2013). For the WALDATEM 2003 and EGER IOP1 (2007) and IOP2 (2008) field campaigns (Chap. 1) at the Waldstein site, the wavelet detection algorithm described in Sect. 6.2.1 was run in the field in a quasi-online fashion to facilitate interpretation of the vertical and horizontal exchange.

6.3 Results and Discussions

6.3.1 Exchange Regimes for Vertical Coupling

It is conceivable to use two alternative approaches for the definition of exchange regimes from coherent structures analysis to indicate a coupling or decoupling between individual levels: the first approach is based upon the comparison of time-averaged flow statistics such as variances and covariances across levels in combination with the assumption that a coupled state requires coherent structures to contribute equally to the total flux at all levels (Thomas and Foken 2007a). Alternatively, one could track single coherent structures in signal traces across the vertical and horizontal to determine their penetration depth from their lagged moment of occurrence to infer mass and energy transport and thus coupling (Zeeman et al. 2013). Here, we will focus on the former since it was originally developed from observations at the Waldstein experimental site and has been used extensively to interpret the transport of passive and chemically reactive trace gases in the canopy layer.

A comparison of the flux contribution of the sweep and ejection phases across several observational levels in the canopy layer can be used to determine coupling or exchange regimes across the vertical (Thomas and Foken 2007a) or horizontal dimension (Serafimovich et al. 2011). Defining exchange regimes following the

statistical approach for conditionally sampled coherent structures requires the assumption that the flux contributed by coherent structures F_{cs} should be equal or similar throughout the portion of the canopy controlled by the coherent exchange. Furthermore, one may invert this argument and define levels as being decoupled if they show a significantly different flux contribution F_{cs} . In a strict sense, this assumption is valid solely for the momentum transfer as its only source is located above the canopy. For scalars, the canonical distribution of sinks and sources may alter the local height-dependent flux (Katul et al. 1995; Ruppert et al. 2006). However, one can argue that a single coherent structure can be interpreted as one spatially cohesive motion transporting momentum and scalars across the depth of the canopy. It may thus transport against local gradients arising from local sinks and sources and force the communication of air across the vertical and horizontal dimension. This may be particularly true for the strong sweep phase, which dominates the transport within the canopy (Thomas and Foken 2007b). Therefore, the coherent exchange F_{cs} is expected to be less prone to modification of local sinks and sources than the total flux.

Based upon the turbulence observations from five levels in a vertical profile during the WALDATEM-2003 experiment, Thomas and Foken (2007a) proposed five distinctly different exchange regimes, which are listed below in order of increasing vertical coupling (see Fig. 6.3).

Wave Motion (Wa) The flow above the canopy is dominated by linear wave motion rather than by turbulence. These periods can be determined from the angle in the phase spectrum between the velocity component and scalar (Cava et al. 2004; Thomas and Foken 2007b). As linear waves usually produce very low to zero scalar flux, the vertical mass flux is assumed to be negligible and thus the above-canopy level to be decoupled from levels below.



Fig. 6.3 Conceptual depiction of the vertical exchange regimes in order of increasing degree of vertical coupling (*left to right*, adapted from Göckede et al. 2007) with kind permission © Authors 2007, CC License 4.0, All rights reserved: Wave motion, Decoupled canopy, Decoupled sub-canopy, Coupled sub-canopy by sweeps, Fully coupled canopy

Decoupled Canopy (Dc) The mass and energy transfer above the canopy is decoupled from that in the crown and sub-canopy. The flux contribution of the sweep and ejection phases between the above-canopy and within-canopy levels are opposite in sign. In general, there is no coherent transport of energy and matter into or out of the canopy.

Decoupled Sub-canopy (Ds) The above-canopy air communicates with the air in the crown layer, but the flux is decoupled from that in the sub-canopy. The region of coherent exchange is limited to the canopy, as the flux contribution of sweeps and ejections at the lower portion of the canopy and the sub-canopy is either opposite in sign or negligible.

Coupled Sub-canopy by Sweeps (Cs) Only the strong sweep motions force the mass and energy exchange between the above-canopy and sub-canopy layers. The flux contributions during the ejection phase between these two levels are either negligible or opposite in sign. This regime is a typical transition regime between Ds and C.

Fully Coupled Canopy (C) Coherent structures communicate across the entire depth of the roughness sublayer including the above-canopy, canopy, and the sub-canopy layers. Both ejection and sweep phases of coherent structures substantially contribute to the vertical mass and energy exchange.

As an example for the temporal pattern of exchange regimes, a case study over 4 days is presented in more detail (Fig. 6.4). Characteristic for this period is the consistent nocturnal linear wave regime (Wa). The generation was facilitated by (i) the strong radiative cooling leading to large negative buoyancy fluxes and (ii) a direction of the flow approaching over some hills southeast of the Waldstein (Thomas and Foken 2007b). The assigned exchange regime suggests a vertical decoupling between within-canopy and above-canopy air (Wa, Dc). Note that the relative flux contribution for scalars seems to increase during these regimes while it remains constant for momentum. However, large pseudo fluxes can be created by linear waves passing through a sensor fixed in space since the vector and scalar time series are phase-shifted but tightly correlated without actually inducing energy and mass transfer. During the day, the strong solar radiation in concert with moderate longitudinal winds ($<3.5 \text{ ms}^{-1}$ above the canopy) results in unstable stratification and vigorous thermally driven turbulence. During the first half of the day, the buoyancy flux at the lower portion of the canopy was weaker compared to the levels above supporting the determined regimes Ds and Dc. Only for the second half of the day, the canopy and sub-canopy were temporarily or fully coupled as indicated by the Cs and C regimes. The increase of the relative flux contribution of coherent structures of up to a ratio of 0.5 coincided with the transition of exchange regimes

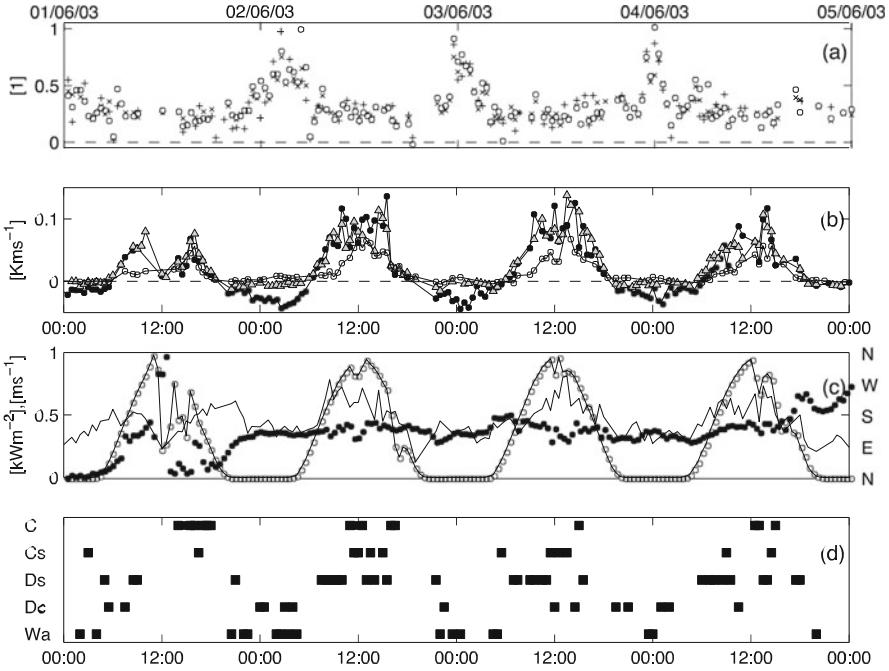


Fig. 6.4 Observations and exchange regimes for the period June 1–3 2003 during the WALDATEM-2003 conducted at the Waldstein experimental site (adapted from Thomas and Foken 2007a, with kind permission © Springer 2007, All rights reserved) (a) Relative flux contribution of coherent structures $F_{cs}F_{tot}^{-1}$ for carbon dioxide (*open circles*), buoyancy (*crosses*), and latent heat (*pluses*) above the canopy. (b) Kinematic buoyancy flux of coherent structures H_{cs} above the canopy (*filled circles*), the canopy top (*gray triangles*), and within the crown layer (*open circles*). (c) Friction velocity (*solid line*), incoming shortwave radiation (*open circles*), and wind direction (*filled circles*) above the canopy. (d) Characterization of the exchange regimes

from Dc to Ds. We presume that this moment may also coincide with the flushing of carbon dioxide-enriched air accumulated over the night. These flushing events were consistently preceded by a low net total flux contribution of coherent structures $F_{cs} = F_{sw} + F_{ej}$ with the sweep and ejection phases having flux contributions of similar magnitude but opposite sign. Sweeps transporting carbon dioxide-enriched air down into the canopy and ejections transporting carbon dioxide-enriched air accumulated during the night out of the sub-canopy lead to a vanishing net flux, while the mass transport and thus coupling are significant. The determination of exchange regimes therefore requires distinguishing between the sweep and ejection phases, while exchange regimes solely based upon the total net coherent flux may be misleading and unphysical.

6.3.2 Exchange Regimes for Horizontal Coupling

Serafimovich et al. (2011) extended the concept of vertical exchange regimes to the horizontal by analyzing observations from a horizontal transect of stations during the EGER experiment. Instead of evaluating the statistical contribution of the sweep and ejection phases to the vertical buoyancy flux across different levels, these horizontal exchange regimes utilize the horizontal flux contribution of the sweep and ejection phases to the buoyancy flux separated into an along-slope and cross-slope component. A linear model with slope α fitted to the flux contribution across an along- and cross-slope transects of stations is used as a reference.

Horizontally Coupled State (C_h) The flux contribution of both sweep and ejection phases is equal to or larger than the slope α . The mass and energy exchange between the transect station is considered to be coupled and air to communicate horizontally.

Horizontally Decoupled State (Dc_h) The flux contribution of both the sweep and ejection phases is either smaller than the reference α or opposite in sign. This state indicates a decoupled coherent mass and energy transport along the transect.

Figure 6.5 gives an example of analyzing both the vertical and horizontal exchange regimes for a 5-day period during the EGER experiment. At night, the airflow in the canopy and above-canopy layers is dominated by wave motions, which suggests a consistent decoupling. During the daylight hours, a full coupling or temporary coupling by sweeps was observed, with the transition periods indicating a partial coupling only. In contrast to the pronounced diurnal cycle of the vertical coupling, the horizontal coupling in the sub-canopy does not show any diurnal pattern but a distinct directional dependence. Cross-slope coupling was more often observed than along-slope coupling, which may be related to the fact that the cross-slope transect was aligned with the mean wind direction.

In a next step, Serafimovich et al. (2011) combined the information about both the horizontal and vertical exchange regimes into defining three general categories describing the bulk two-dimensional coupling:

Horizontal and Vertical Decoupling The sub-canopy is decoupled horizontally (Dc_h) indicating significantly different contribution of coherent structures to the horizontal turbulent fluxes across the transect. The sub-canopy flux is decoupled from the canopy and above-canopy layers (Dc , Ds). Coherent structures do not communicate momentum and mass across the canopy.

Horizontal Decoupling with Vertical Coupling Coherent structures penetrate deeply into the canopy causing a vertical communication of air, while they do not contribute to horizontal transport.

Full Horizontal and Vertical Coupling The sub-canopy air is coupled with that in the canopy and above-canopy air while coherent structures also force the horizontal communication of air. Coherent structures penetrate deeply into the canopy while they also propagate longitudinally.

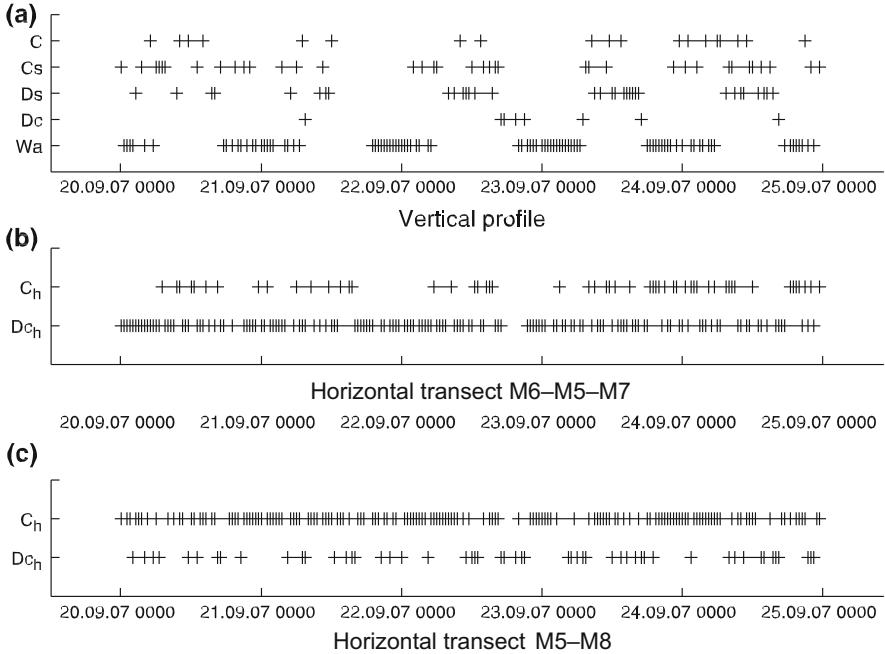


Fig. 6.5 Exchange regimes during a 5-day period during the EGER experiment at the Waldstein-Weidenbrunnen site (Adapted from Serafimovich et al. (2011) with kind permission © Springer 2011, All right reserved) across (a) the vertical profile covering the above-canopy, canopy, and sub-canopy layers, (b) the horizontal along-slope transect, and (c) the horizontal cross-slope transect. The ordinates denote the following exchange regimes: C, full coupling; Cs, coupling by sweeps; Ds, decoupled sub-canopy; Dc, decoupled canopy; Wa, wave motion; C_h , horizontally coupled sub-canopy layer; and D_{ch} , horizontally decoupled sub-canopy layer

Applying this bulk 2-D classification system of the exchange to the observations yielded that the full horizontal and vertical coupling was observed more often for the along-wind than the cross-wind component of the horizontal coupling regime (See Fig. 8 and Table 3 in Serafimovich et al. 2011). This observation matches well with the notion that the mixing-layer coherent structures are vertically deep motions with a scale of approximately twice the canopy height and evolve and penetrate into the canopy as they propagate with the mean wind. As a result, these coherent structures appear as streaks in large eddy simulations when viewed from above (Kanani-Suhring and Raasch 2015). If the station spacing in the cross-wind direction exceeds that of the cross-wind length scale of the coherent structure, then these structures may not contribute spatially equal to the mass and energy transfer in the sub-canopy layer. In fact, when viewed in a coordinate system moving with the mean convective velocity at the canopy top, the pressure field may create quiescent buffer zones of low-velocity or stagnant air between the higher-velocity fluid pockets of the sweeps, which separate individual coherent structures from each other.

6.3.3 Implementation for Quantifying Daytime Sub-canopy Respiration

Thomas et al. (2008) developed a mathematical formulation for the calculation of the daytime respiration flux from high-frequency eddy-covariance data building upon a conceptual framework proposed by Scanlon and Albertson (2001). It is based upon conditionally sampling data organized into quadrants (e.g., Shaw et al. 1983). This method uses a modified relaxed eddy accumulation approach originally proposed by Businger and Oncley (1990) in combination with a hyperbolic threshold. The main assumption of the Thomas et al. (2008) method is that respiration signals originating in the sub-canopy carry a unique identifiable signature in the scalar-scalar cross-correlation between CO₂ and water vapor, which is maintained as they are transported through the canopy. This signature is distinguishable from other sinks and sources and allows for conditional sampling of the respiration signal and the calculation of a sub-canopy respiration CO₂ flux during daytime conditions. These respiration signals appear as excursions from the similarity-theory predictions for an actively photosynthesizing and transpiring plant canopy. Coherent structures play a key role in preserving this unique sub-canopy scalar-scalar fingerprint as only this flow mode can transport air vertically through the canopy in a coherent fashion on time scales short enough to avoid significant mixing with the air carrying the different scalar-scalar fingerprint of the main tree crown.

Combining the vertical coherent exchange regimes with the daytime respiration analysis yielded that the correlation coefficient between CO₂ and water vapor was found to be strongly negative with $r_{c,q} \approx -0.60$ for the fully coupled exchange regime (C) during daytime conditions. The signals progressively decorrelated with decreasing vertical coupling from exchange regime Cs to Dc and eventually arrived at a positive correlation of $r_{c,q} \approx 0.35$ for the Wa regime. A strongly negative correlation indicates that the scalar-scalar fingerprint of the tree crown dominates and that mixing is sufficiently strong to integrate overall sinks and sources in agreement with the definition of the C regime. In contrast, a positive correlation indicates that vertical mixing is negligible, which agrees with the definition of the Dc and Wa regimes.

Thomas et al. (2008) concluded that the method produces meaningful daytime estimates of sub-canopy respiration in stands of low and moderate density with little understory and negligible sub-canopy photosynthesis and fails in dense and multi-layered canopies such as the Waldstein-Weidenbrunnen site. To evaluate this conclusion, the method was applied to the EGER IOP1 (2007) data set collected at the turbulence tower in whose vicinity the forest is less dense (Chap. 2). The key difference between this and the original study for the Waldstein-Weidenbrunnen site (Thomas et al. 2008) was the application of a smaller $r_{c,q}$ threshold for the selection of respiration events as the decorrelation between CO₂ and water vapor was generally low.

An example of the quadrant analysis is shown in Fig. 6.6 separated for day- and nighttime conditions. For the 23 m observational level, the diurnal pattern in

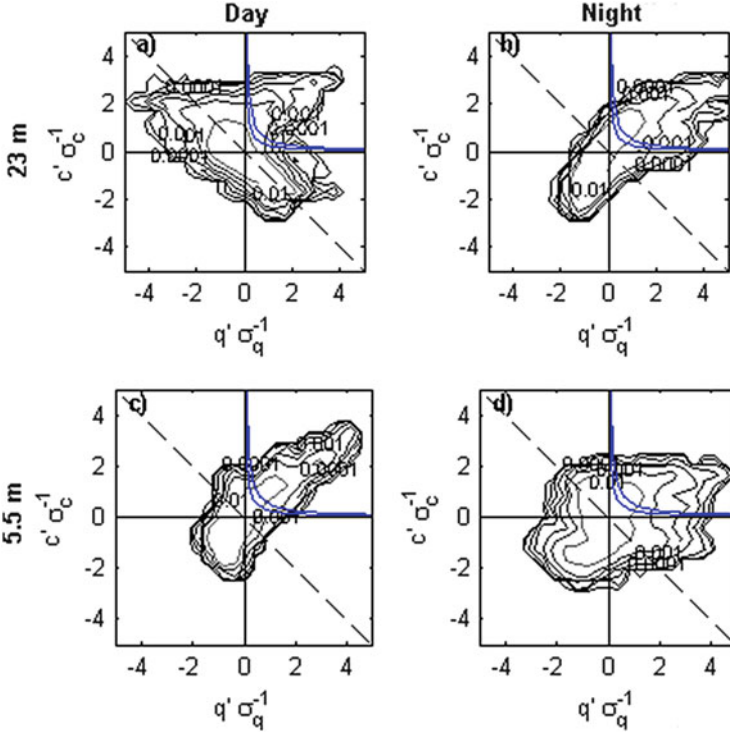


Fig. 6.6 Scalar probability density contour plots of normalized c' and q' fluctuations for daytime and nighttime conditions. (a), (c): September 21, 2007—13:30 to 14:00 h at 23 m and 5.5 m, respectively. (b), (d): September 21, 2007—22:00–22:30 h at 23 m and 5.5 m, respectively. The dashed line indicates a $-1:1$ relationship. Hyperbolic thresholds of $H = 0.25$ (inner) and $H = 0.5$ (outer) for the first quadrant are also shown

the scalar-scalar correlation agrees with that originally proposed by Thomas et al. (2008) switching signs during transition from the light to dark regime. In contrast, the data observed at 5.5 m show no diurnal change, which indicates that respiration is the dominant process in the sub-canopy. A good agreement between respiration estimates from the modified REA method and an independent Arrhenius-type model parameterized using nighttime data was found for the above-canopy observations (Fig. 6.7). In spite of the agreement, several limitations were found. During daytime conditions and especially around noon, the respiration signal becomes very weak and difficult to detect most likely because of the increased mixing during intense convective forcing of the turbulence. The vanishing respiration signals lead to gaps in the time series, which will need to be addressed. Other shortcomings include the model used to compute the proportionality factor in the REA formulation and the lack of an objective criterion to determine the hyperbolic threshold criterion (H). The method will fail for conditions when the $r_{c,q}$ is positive as found for the sub-canopy observations. Therefore, the method is restricted to systems close to the

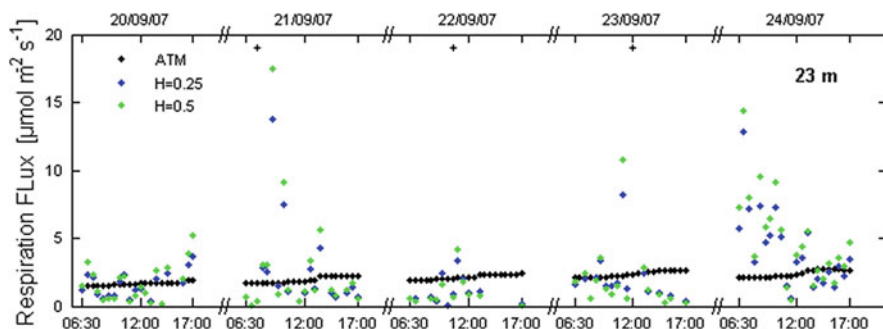


Fig. 6.7 Daytime respiration flux estimated at 23 m height. Fluxes are calculated by a conditional hyperbolic REA sampling with $H = 0.25$ (blue) and 0.5 (green). Each data point represents a 30-minute interval. The black line indicates the flux estimates derived by an Arrhenius-type model (ATM—Subke et al. 2004). Black crosses mark at the top indicate low data quality (Quality flag of 7–8 according to Foken et al. 2004)

canopy height. Nonetheless, this method provides a viable alternative to compute independent estimates of daytime respiration not available from the classical eddy-covariance method that can be utilized for comparison with extrapolating the nighttime fluxes using a simple temperature model. Thomas et al. (2013) showed that applying this method to compute the sub-canopy respiration as an indirect method to account for advective respiration losses under conditions of a decoupled sub-canopy significantly improves the annual net exchange estimate (NEE) for carbon by enhancing ecosystem respiration by up to 63 % (from 1233 to 2009 $\text{gC m}^{-2} \text{yr}^{-1}$).

6.3.4 Implications for Spatial Heterogeneity of Sub-canopy Carbon Dioxide Concentrations, Gradients, and Horizontal Advection

The previous sections demonstrated that coherent structures are a major flow mode controlling the transport of air across the canopy volume. If one assumes that the penetration depth and strength of coherent structures depend on the local density of plant biomass, i.e., the architecture of the forest, acting as an efficient sink for momentum, then it is conceivable that the spatial variation of biomass creates a similarly variable pattern in coherent air exchange. Since the vertical gradient of CO_2 in forests is steep with differences between the forest floor and above the canopy amounting to several hundred parts per million, we hypothesize that the horizontal variability of the vertical coherent air exchange may create systematic pockets of lower and higher CO_2 concentration in the sub-canopy as a result of the varying degrees of mixing. These pockets then define stationary, i.e., temporally,

invariant gradients that may lead to significant and systematic horizontal advection when multiplied with a nonzero mean advective sub-canopy velocity. Hence, the forest canopy architecture itself may be an important driver for the spatial variability of the contribution of the individual terms of the canopy mass balance. To our knowledge, this phenomenon has not been included in the discussion of sub-canopy scalar and particularly CO₂ exchange, which is traditionally thought to be controlled by soil respiration rates and soil composition, temperature, and moisture (Staebler and Fitzjarrald 2004) or by gravitationally driven density currents on sloped surfaces (Aubinet et al. 2003). Similar investigations were done during The EGER field campaigns in 2007 and 2008 (Siebicke et al. 2012).

To test this hypothesis, the plant area index (PAI) as a relative measure of vertically integrated canopy density (Fig. 6.8) and its spatial gradient (Fig. 6.9) were mapped and compared against the sub-canopy CO₂ concentrations sampled in ten discrete locations indicated by the black dots (Fig. 6.10). It is evident that air sampled at one higher PAI location was relatively enriched (M5, Fig. 6.10b, for location numbers see Fig. 6.8) compared against that at a lower PAI site (M13, Fig. 6.10a) for dynamically stable stratification evaluated above the canopy. Here CO₂ concentrations were relatively depleted throughout the diurnal period. A possible explanation for the stationary high-CO₂ pockets is the limited turbulent diffusion which includes the coherent transport that may enhance the canopy density effects. A consistent relationship between PAI and mean CO₂ concentration perturbation for all ten sampling locations in the sub-canopy could not be established though; however, it was found that sampling locations with large PAI gradient (Fig. 6.7) – like M13 – had the longest duration and strongest amplitude of coherent structures similar to those found at the forest edge (Eder et al. 2013). Note, however, that the results for the two selected locations shown in Fig. 6.10 represent a large number of samples and thus lend some preliminary support to our initial hypothesis. Even though canopy density may be important in defining stationary scalar gradients and coherent transport, other drivers such as orientation of the local slope in relation to the direction of the approaching flow, variations in the above-canopy wind velocity, and the distribution of shortwave radiation, nutrients, and understory vegetation may exert additional control on the sub-canopy CO₂ transport. These results prompt future research at this site to include spatially explicit information about all potential drivers to establish causality and gain a mechanistic understanding.

6.4 Conclusions

The field experiments conducted at the Waldstein experimental site made a significant contribution to our understanding of the transport at the forest canopy air interface. Synthesizing the results from several intensive field campaigns conducted over a period of more than two decades prompts us to draw a set of general conclusions:

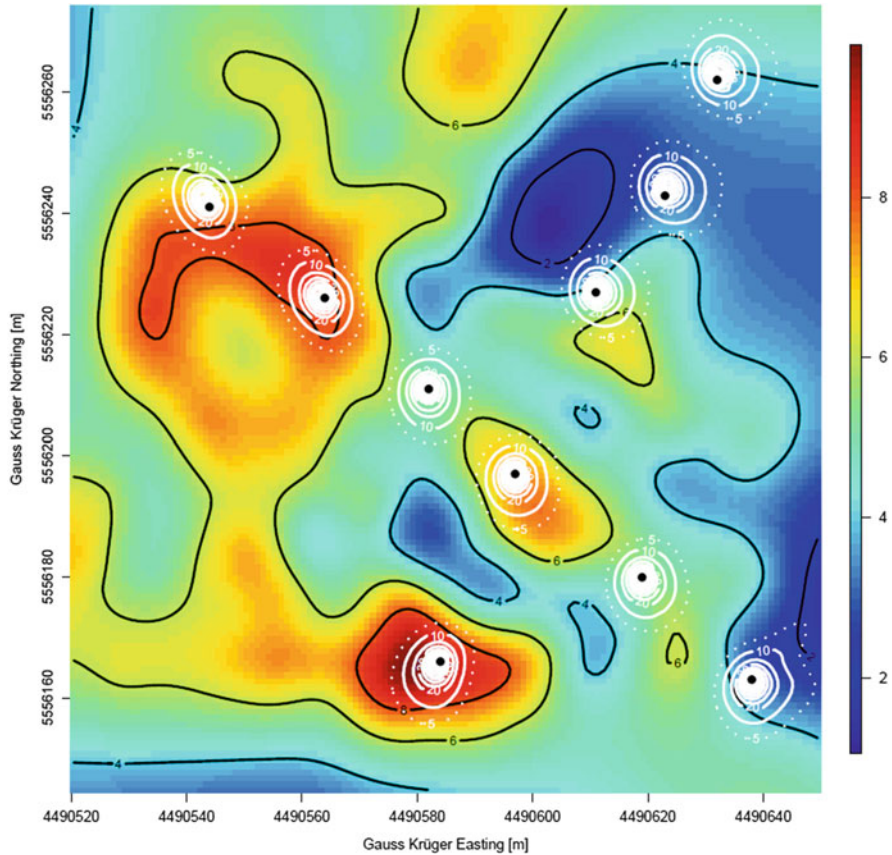


Fig. 6.8 Map of the plant area index (PAI) given as colors with *black* contour lines in a Gauss-Krueger coordinate system. *Black dots* indicate the positions of the sub-canopy air inlets (from NW to SE: M10, M11, M12, M5, M9, M8; from NE to SW: M14, M13, M6, M5, M7). *White isolines* are the relative contribution to the local footprint for stable stratification with a contour spacing of 10 %. The outermost area encloses the area from which 95 % of the flux originates. Raw PAI from E. Falge (pers.com.). Measurements were conducted during the EGER IOP1 experiment in 2007 (Siebicke 2011, published with kind permission of © Author 2011, All rights reserved)

- The vertical exchange regimes determined based upon the mean flux contribution of the sweep and ejection phases of the coherent structures (Thomas and Foken 2007a), which were observed across several vertical layers in the forest canopy, are physically and biologically meaningful. They offer means to diagnosing the degree and depth of the vertical coupling, which is crucial for the quality control and interpretation of trace gas and energy fluxes from tall vegetation (see also Chap. 12).
- The analysis of the coherent forest air exchange is key to understanding the fluxes of reactive trace gases and particulate matter (Foken et al. 2012; Chaps. 8 and 9)

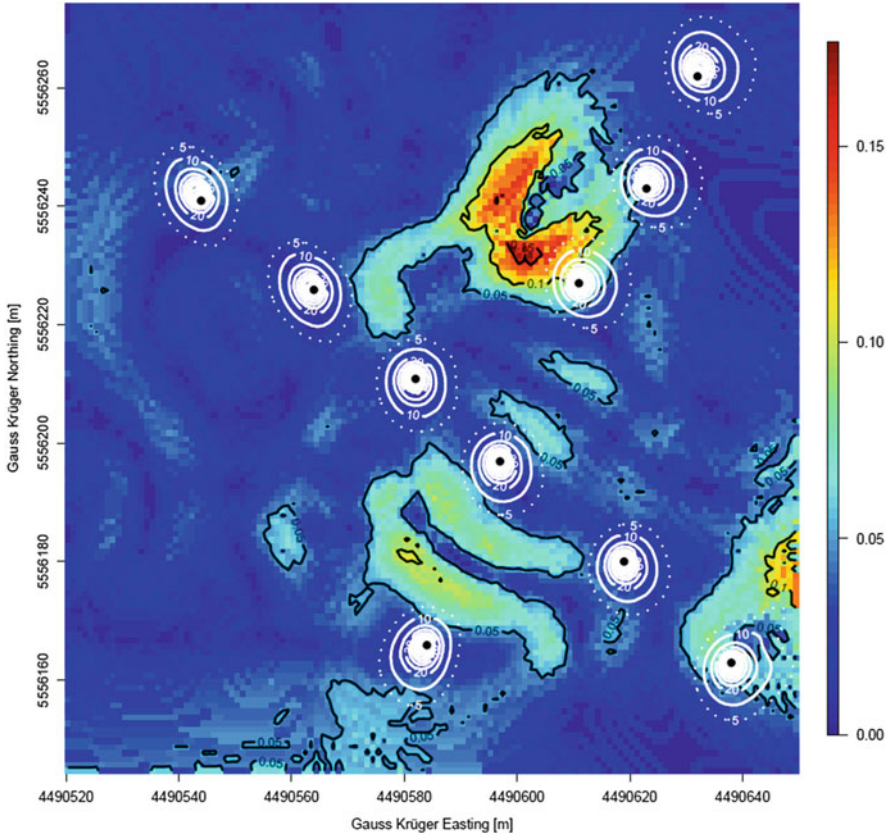


Fig. 6.9 Spatial gradients of PAI [$\text{m}^2 \text{m}^{-2} \text{m}^{-1}$] of the data displayed in Fig. 6.6

as they exert an important control on the Damköhler number, which is defined as the ratio of the transporting time scale to that of the chemical reaction.

- Evaluating the full three-dimensional carbon and energy balance for a forest volume, which includes the vertical and horizontal flux divergences and advective component, requires a careful investigation of the degree of horizontal coupling along the direction of the mean mass flow (Serafimovich et al. 2011).
- The spatial distribution of plant biomass including leaf area may create stationary sub-canopy scalar gradients by exerting a systematic control on the penetration depth and horizontal movement of coherent structures. There is some support that transition areas from low to high PAI may be prone to strong vertical coherent transport and mixing of CO_2 -depleted above-canopy air into the sub-canopy. However, these gradients lead to horizontal advection only if the horizontal mass flow is aligned with their spatial orientation.
- The analysis of advective mass transport without a detailed investigation of the coherent transport across the horizontal and the vertical may lead to a

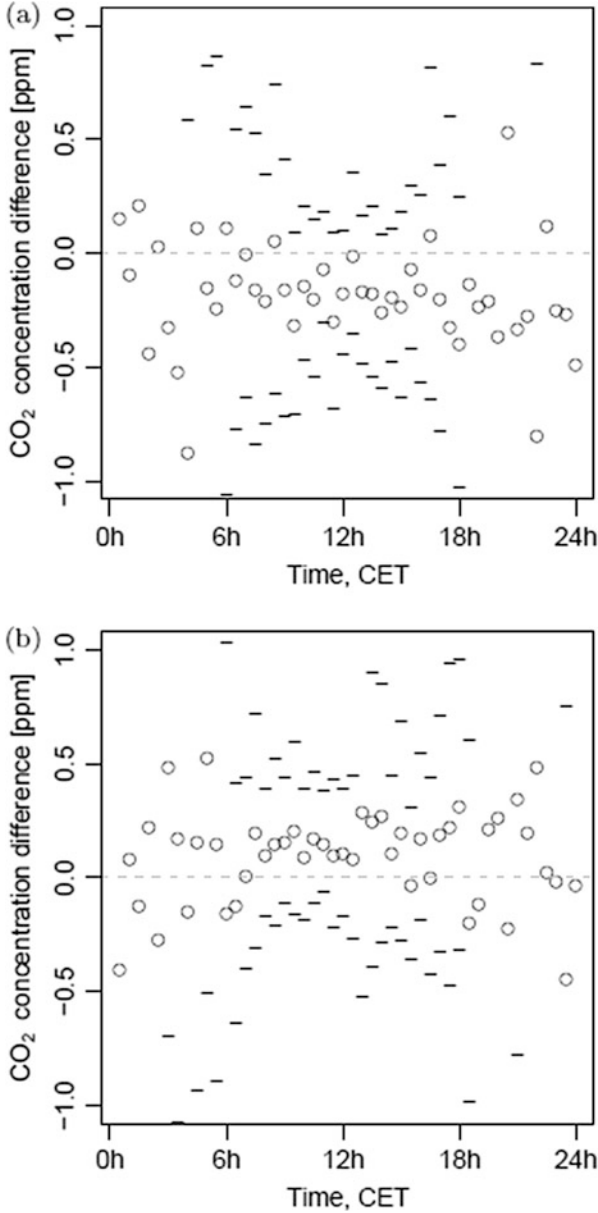


Fig. 6.10 Mean diurnal cycle of local CO₂ concentration perturbations for (a) a sample location with a low representative PAI (M13) and (b) a high representative PAI (M5). Circles depict the mean, dashes the standard deviation of the individual 30-minute intervals. Number of observations: 1181 spanning the period 11th of June to 13th of July, 2008. For locations of stations M13 and M5, see caption of Fig. 6.6. (Siebicke 2011, published with kind permission of © Author 2011, All rights reserved)

misinterpretation of the observations (Aubinet et al. 2010), since horizontal decoupling and limited vertical mixing frequently coincide, particularly in higher PAI stands.

In spite of the significant progress in detecting, extracting, and quantifying coherent structures and understanding their role for vertical and horizontal exchange and coupling regimes, many questions remain open. From our perspective, the most pressing questions are connected to elucidating the links between spatial heterogeneity of the surface architecture and the spatiotemporal variability of the forest flow modes and forest mass and scalar transport. Explicit spatial information over several orders of magnitude from decimeter to hundreds of meters is required here to advance this field of research. To this end, the recently developed spatially continuous quasi three-dimensional sensing technology of fiber-optic distributed temperatures sensing (DTS) may offer novel experimental insights at the field scale (Thomas et al. 2012; Sayde et al. 2015). This technology is capable of sensing air temperature and wind speed at submeter resolution over a distance of hundreds of meters with a temporal resolution of seconds. It has the potential to yield the observations necessary to better diagnose energy and mass transport in the roughness-sublayer transport. An advantage of the spatially resolving information from DTS is that it eliminates the need for strong assumptions such as ergodicity, Taylor's hypothesis of frozen turbulence, and scaling laws such as the convective velocity scale (Finnigan 1979; Shaw et al. 1995).

References

- Adrian RJ (2007) Hairpin vortex organization in wall turbulence. *Phys Fluids*. doi:10.1063/1.2717527
- Antonia RA, Browne LWB, Bisset DK, Fulachier L (1987) A description of the organized motion in the turbulent far wake of a cylinder at low Reynolds numbers. *J Fluid Mech* 184:423–444
- Aubinet M, Feigenwinter C, Heinesch B et al (2010) Direct advection measurements do not help to solve the night-time CO₂ closure problem: evidence from three different forests. *Agric For Meteorol* 150:655–664
- Aubinet M, Heinesch B, Yernaux M (2003) Horizontal and vertical CO₂ advection in a sloping forest. *Bound Lay Meteorol* 108:397–417
- Bergström H, Högström U (1989) Turbulent exchange above a pine forest. II. Organized structures. *Bound Lay Meteorol* 49:231–263
- Brunet Y, Collineau S (1994) Wavelet analysis of diurnal and nocturnal turbulence above a maize canopy. In: Foufoula-Georgiou E, Kumar P (eds) *Wavelets in geophysics*. Academic Press, San Diego, pp 129–150
- Businger JA, Oncley SP (1990) Flux measurement with conditional sampling. *J Atmos Ocean Technol* 7:349–352
- Cava D, Giostra U, Siqueira M, Katul G (2004) Organised motion and radiative perturbations in the nocturnal canopy sublayer above an even-aged pine forest. *Bound Lay Meteorol* 112:129–157
- Chen J, Hu F (2003) Coherent structures detected in atmospheric boundary-layer turbulence using wavelet transforms at Huaihe River Basin, China. *Bound Lay Meteorol* 107:429–444
- Collineau S, Brunet Y (1993) Detection of turbulent coherent motions in a forest canopy. Part I: wavelet analysis. *Bound Lay Meteorol* 65:357–379

- Eder F, Serafimovich A, Foken T (2013) Coherent structures at a forest edge: properties, coupling and impact of secondary circulations. *Bound Lay Meteorol* 148:285–308
- Finnigan JJ (1979) Turbulence in waving wheat. II. Structure of momentum transfer. *Bound Lay Meteorol* 16:213–236
- Foken T, Göckede M, Mauder M, Mahrt L, Amiro BD, Munger JW (2004) Post-field data quality control. In: Lee X et al (eds) *Handbook of micrometeorology: a guide for surface flux measurement and analysis*. Kluwer, Dordrecht, pp 181–208
- Foken T, Meixner FX, Falge E et al (2012) Coupling processes and exchange of energy and reactive and non-reactive trace gases at a forest site—results of the EGER experiment. *Atmos Chem Phys* 12:1923–1950. doi:[10.5194/acp-12-1923-2012](https://doi.org/10.5194/acp-12-1923-2012)
- Gao W, Shaw RH, Paw U KT (1989) Observation of organized structures in turbulent flow within and above a forest canopy. *Bound Lay Meteorol* 47:349–377
- Göckede M, Thomas C, Markkanen T et al (2007) Sensitivity of Lagrangian Stochastic footprints to turbulence statistics. *Tellus B* 59:577–586. doi:[10.1111/j.1600-0889.2007.00275.x](https://doi.org/10.1111/j.1600-0889.2007.00275.x)
- Hommema SE, Adrian RJ (2003) Packet structure of surface eddies in the atmospheric boundary layer. *Bound Lay Meteorol* 106:147–170
- Howell JF, Mahrt L (1997) Multiresolution flux decomposition. *Bound Lay Meteorol* 83:117–137
- Kallistratova MA, Kouznetsov RD (2004) Systematization of experimental data on forms and scales of coherent structures in the atmosphere. In: 12th international symposium on acoustic remote sensing, Cambridge
- Kanani-Suhring F, Raasch S (2015) Spatial variability of scalar concentrations and fluxes downstream of a clearing-to-forest transition: a large-eddy simulation study. *Bound Lay Meteorol* 155:1–27. doi:[10.1007/s10546-014-9986-3](https://doi.org/10.1007/s10546-014-9986-3)
- Katul G, Goltz SM, Hsieh CI et al (1995) Estimation of surface heat and momentum fluxes using the flux-variance method above uniform and non-uniform terrain. *Bound Lay Meteorol* 80:249–282
- Kumar P, Foufoula-Georgiou E (1994) Wavelet analysis in geophysics: an Introduction. In: Foufoula-Georgiou E, Kumar P (eds) *Wavelets in geophysics*. Academic Press, San Diego, pp 1–43
- Lykossov VN, Wamser C (1995) Turbulence intermittency in the atmospheric surface layer over snow-covered sites. *Bound Lay Meteorol* 72:393–409
- Paw U KT, Brunet Y, Collineau S et al (1992) Evidence of turbulent coherent structures in and above agricultural plant canopies. *Agric For Meteorol* 61:55–68
- Poggi D, Porporato A, Ridolfi L et al (2004) The effect of vegetation density on canopy sub-layer turbulence. *Bound Lay Meteorol* 111:565–587
- Raupach MR, Finnigan JJ, Brunet Y (1996) Coherent eddies and turbulence in vegetation canopies: the mixing-layer analogy. *Bound Lay Meteorol* 78:351–382
- Ruppert J, Thomas C, Foken T (2006) Scalar similarity for relaxed eddy accumulation methods. *Bound Lay Meteorol*: 39–63. doi:[10.1007/s10546-005-9043-3](https://doi.org/10.1007/s10546-005-9043-3)
- Sayde C, Thomas CK, Wagner J, Selker JS (2015) High-resolution wind speed measurements using actively heated fiber optics. *Geophys Res Lett* 42:10,064–10,073. doi:[10.1002/2015GL066729](https://doi.org/10.1002/2015GL066729)
- Scanlon TM, Albertson JD (2001) Turbulent transport of carbon dioxide and water vapor within a vegetation canopy during unstable conditions: identification of episodes using wavelet analysis. *J Geophys Res D* 106:7251–7262
- Serafimovich A, Thomas CK, Foken T (2011) Vertical and horizontal transport of energy and matter by coherent motions in a tall spruce canopy. *Bound Lay Meteorol* 140:429–451. doi:[10.1007/s10546-011-9619-z](https://doi.org/10.1007/s10546-011-9619-z)
- Shaw RH, Brunet Y, Finnigan JJ, Raupach MR (1995) A wind tunnel study of air flow in waving wheat: two-point velocity statistics. *Bound Lay Meteorol* 76:349–376
- Shaw RH, Paw U KT, Gao W (1989) Detection of temperature ramps and flow structures at a deciduous forest site. *Agric For Meteorol* 47:123–138
- Shaw RH, Tavangar J, Ward DP (1983) Structure of the reynolds stress in a canopy layer. *J Clim Appl Meteorol* 22:1922–1931

- Siebicke L (2011) Advection at a forest site—an updated approach. PhD Thesis, University of Bayreuth, Bayreuth, 113 pp
- Siebicke L, Hunner M, Foken T (2012) Aspects of CO₂-advection measurements. *Theor Appl Climatol* 109:109–131
- Staebler RM, Fitzjarrald DR (2004) Observing subcanopy CO₂ advection. *Agric For Meteorol* 122:139–156. doi:[10.1016/j.agrformet.2003.09.011](https://doi.org/10.1016/j.agrformet.2003.09.011)
- Subke J-A, Buchmann N, Tenhunen JD (2004) Soil CO₂ fluxes in spruce forests—temporal and spacial variation, and environmental controls. In: Matzner E (ed) *Biogeochemistry of forested catchments in a changing environment, a German case study*. Ecological studies, vol 172. Springer, Berlin, pp 127–141
- Thomas CK (2011) Variability of subcanopy flow, temperature, and horizontal advection in moderately complex terrain. *Bound Lay Meteorol* 139:61–81. doi:[10.1007/s10546-010-9578-9](https://doi.org/10.1007/s10546-010-9578-9)
- Thomas C, Foken T (2005) Detection of long-term coherent exchange over spruce forest using wavelet analysis. *Theor Appl Climatol* 80:91–104. doi:[10.1007/s00704-004-0093-0](https://doi.org/10.1007/s00704-004-0093-0)
- Thomas C, Foken T (2007a) Flux contribution of coherent structures and its implications for the exchange of energy and matter in a tall spruce canopy. *Bound Lay Meteorol* 123:317–337. doi:[10.1007/s10546-006-9144-7](https://doi.org/10.1007/s10546-006-9144-7)
- Thomas C, Foken T (2007b) Organised motion in a tall spruce canopy: temporal scales, structure spacing and terrain effects. *Bound Lay Meteorol* 122:123–147. doi:[10.1007/s10546-006-9087-z](https://doi.org/10.1007/s10546-006-9087-z)
- Thomas CK, Kennedy AM, Selker JS et al (2012) High-resolution fibre-optic temperature sensing: a new tool to study the two-dimensional structure of atmospheric surface layer flow. *Bound Lay Meteorol* 142:177–192. doi:[10.1007/s10546-011-9672-7](https://doi.org/10.1007/s10546-011-9672-7)
- Thomas C, Martin JG, Goeckede M et al (2008) Estimating daytime subcanopy respiration from conditional sampling methods applied to multi-scalar high frequency turbulence time series. *Agric For Meteorol* 148:1210–1229. doi:[10.1016/J.Agrformet.2008.03.002](https://doi.org/10.1016/J.Agrformet.2008.03.002)
- Thomas CK, Martin JG, Law BE, Davis K (2013) Toward biologically meaningful net carbon exchange estimates for tall, dense canopies: multi-level eddy covariance observations and canopy coupling regimes in a mature Douglas-fir forest in Oregon. *Agric For Meteorol* 173:14–27. doi:[10.1016/j.agrformet.2013.01.001](https://doi.org/10.1016/j.agrformet.2013.01.001)
- Thomas C, Mayer J-C, Meixner FX, Foken T (2006) Analysis of low-frequency turbulence above tall vegetation using a Doppler sodar. *Bound Lay Meteorol* 119:563–587. doi:[10.1007/s10546-005-9038-0](https://doi.org/10.1007/s10546-005-9038-0)
- Vickers D, Mahrt L (1997) Quality control and flux sampling problems for tower and aircraft data. *J Atmos Ocean Technol* 14:512–526
- Wilczak JM, Oncley SP, Stage SA (2001) Sonic anemometer tilt correction algorithms. *Bound Lay Meteorol* 99:127–150
- Zeeman MJ, Eugster W, Thomas CK (2013) Concurrency of coherent structures and conditionally sampled daytime sub-canopy respiration. *Bound Lay Meteorol* 146:1–15. doi:[10.1007/s10546-012-9745-2](https://doi.org/10.1007/s10546-012-9745-2)
- Zhou J, Adrian RJ, Balachandar S, Kendall TM (1999) Mechanisms for generating coherent packets of hairpin vortices in channel flow. *J Fluid Mech* 387:353–396. doi:[10.1017/S002211209900467X](https://doi.org/10.1017/S002211209900467X)